Leveraging FMCW Radar for Monitoring On-Bed States of Human Presence, Posture, and Motion

Fan, Mingyang

(出版者 / Publisher)
法政大学大学院情報科学研究科

(雑誌名 / Journal or Publication Title)
法政大学大学院紀要. 情報科学研究科編

(巻 / Volume)
19

(開始ページ / Start Page)
1

(終了ページ / End Page)
6

(発行年 / Year)
2024-03-24

(URL)
https://doi.org/10.15002/00030604

Leveraging FMCW Radar for Monitoring On-Bed States of Human Presence, Posture, and Motion

Mingyang Fan
Graduation School of Computer and Information Sciences
Hosei University, Tokyo, Japan
mingyang.fan.8i@stu.hosei.ac.jp

Abstract— **In this study, a non-invasive solution for on-bed monitoring of human states using FMCW radar is proposed. Our unique approach models the bed area and region of interest (ROI) from the radar perspective, projecting them into azimuth-range and elevation-range maps for precise state detection, in which, the Minimum Variance Distortionless Response (MVDR) is used for target localization, Fast Fourier Transform (FFT) and Weighted Range-Time-Frequency Transform (WRTFT) is used for Doppler data extraction. A new method is introduced for on-bed state detection by capitalizing on chest localization within the azimuth-elevation-range-ROI mapping, enhancing detection accuracy, and this method can concurrently monitor on-bed presence, posture, motion, and turning, providing a holistic view of sleep behavior.**

Keywords— FMCW radar, on-bed, detection, presence, motion, posture, angle, range, Doppler.

I. INTRODUCTION

Automatically detecting and accurately logging sleep states occurring while on bed is of great importance for analyzing sleep quality and improving overall health. This is because sleep accounts for nearly one-third of an individual's life. The ability to accurately differentiate between time spent on-bed and off-bed, in addition to detecting posture, and motion in an on-bed setting is fundamental in gaining deeper insights into sleep patterns, improving automatic sleep scoring, and analysis of sleep quality.

The existing methods for presence detection, predominantly relying on cameras [1], [2], [3], and pressure sensors[4], come with several limitations, including privacy concerns, discomfort, and lack of precision. Ideally, a monitoring system operating in such environment and conditions should operate without physical contact, without causing disruption, and functions effectively even in low-light environments commonly encountered during sleep. This led us to consider a solution based on radar technology that meets all the requirements for monitoring on-bed state.

Previous studies on the use of radar technology include an example of such studies is the work published by MIT labs [5] focusing on using radar to capture several types of information from the subject and roughly locate his position in a room setting. A similar study [6] used dual FMCW radars and proposed a solution called Argosleep based on a proposed deep learning architecture to classify the different sleep postures. FMCW radar was also used for posture classification [7][8], sleep stage recognition [9], and to capture vital signs in sleep environment [10]. Our proposed solution effectively addresses the challenges of restricted radar detection, reflections from the surrounding environment, various body postures, and multiple reflection locations. Through the integration of advanced algorithms and precise localization techniques, this work provides an innovative approach that enables accurate and comprehensive on-bed presence, posture, and movement detection. To summarize, this paper makes the following contributions:

- A unique method to model the bed area and the region of interest (ROI) within a sleeping context from the radar perspective. This technique allows for the projection of the bed area and ROI into elevation-range (ER) and azimuth-range (AR) maps.
- A novel solution is introduced for detecting the on-bed state of a subject by leveraging chest localization in the AR-ER-ROI mapping.
- A comprehensive and simultaneous approach for on-bed presence, posture, and motion detection.

The remainder of this paper is organized as follows. Section II showcases our proposed solution highlighting its different modules and detection algorithms, while section III presents the different radar settings and experimental protocols. In Section IV, the evaluation results and discussion about performance and current limitations are presented. In section V, the paper is concluded with a summary and an outline of future work.

II. ON-BED STATE DETECTION MODELING AND METHODS

In this section, a comprehensive overview of the proposed method for detecting presence, movement, and posture based on FMCW radar in an on-bed setting is offered.

A. Model and Projection of the Region of Interest (ROI)

One of the most important steps in our proposal is the modeling of the bed and the region of detection, call Region of Interest (ROI). As shown in Fig. 1, the ROI is a rectangular area that matches the dimensions of the bed in length and width, with a height of 1 meter. When the target falls within the ROI, the target is distinguished to be on the bed. Since radar can only provide range, elevation, and azimuth (r, e, a) information, a conversion between spherical coordinates and Cartesian coordinates is needed. The ROI coordinates (r, e, a) are converted from the (x, y, z) system using equations (1) ~ (3) where H_r is the height of the radar to calculate the corresponding range, elevation, and azimuth values. These values are then plotted on the AR (Azimuth-Range) and ER (Elevation-Range) maps. The (x, y, z) coordinate system is established by taking the radar projection's position on the ground as the origin. In Fig. 1, the red line represents the effective detection range of the ROI in the AR and ER maps, indicating the actual boundaries within which detections are considered. On the other hand, the blue line depicts the projection of the ROI boundary in the AR and ER maps, but it does not serve as the detection range for determining targets.

$$r = \sqrt{x^2 + y^2 + (z - H_r)^2} \tag{1}$$

$$e = \tan^{-1}\left(\frac{y\sin\theta + (z - H_r)\cos\theta}{y\cos\theta - (z - H_r)\sin\theta}\right) \tag{2}$$

$$a = \tan^{-1}\left(\frac{-x}{y\cos\theta - (z - H_r)\sin\theta}\right) \tag{3}$$

Supervisor: Prof. Jianhua Ma

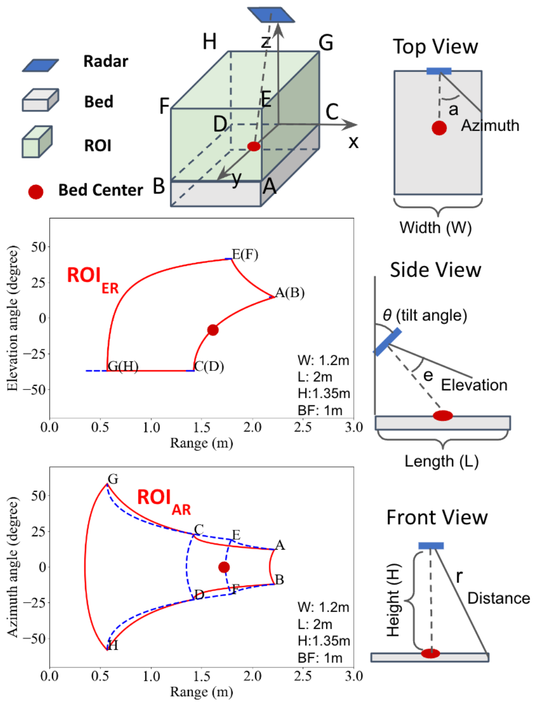

Fig. 1. Bed ROI model and its projections of elevation-range (ER) and azimuth-range (AR) from the view of the radar placed on the head wall.

B. *Processing and Detection Pipeline*

Fig. 2 depicts the processing pipeline adopted in our proposed method. It is layered according to three main levels: data pre-processing, target data extraction, and target state detection.

(1) Data Pre-processing. The initial stage in the processing chain is centered on the acquisition and digital conversion of received radar signals. An Analog-to-Digital Converter (ADC) is used to convert the radar data into a digital format and subsequently, a Fast Fourier Transform (FFT) commonly referred to as 1DFFT (range-FFT) is applied to extract range information. This step allows the segmentation of the collected data into discrete distance intervals, known as 'range bins'. Since radar sends multiple chirps per frame, only one chirp is selected from each frame which still meets the requirements of the proposed solution and further facilitates the data processing and storing in later stages. Finally, clutter removal is used to eliminate reflections from static objects in the environment, such as floors, walls, and furniture.

(2) Target Data Extraction. This part has two main tasks: identifying the location of the target, and extracting movement information within the observed scene. For the former task, The Minimum Variance Distortionless Response (MVDR) algorithm is used to determine the Angle of Arrival (AoA) information. This will enable the precise localization of targets within the radar's field of view by using range-azimuth-elevation coordinates. To enhance the detectability of a target within the scene, a power threshold is set by analyzing the background noise within the scene during the first 10 sec of the recording when the scene is empty (calibration process). Next, the Cell Averaging - Constant False Alarm Rate (CA-CFAR) algorithm is applied to further distinguish the most significant sources of power and output filtered azimuth-range (AR) and elevation-range (ER) maps shown in Fig. 3 (left). Then Weighted Range-Time-Frequency Transform (WRTFT) [9] is applied to AR and ER maps with time. The final output of this step is the weighted range (WR) AT and ET maps.

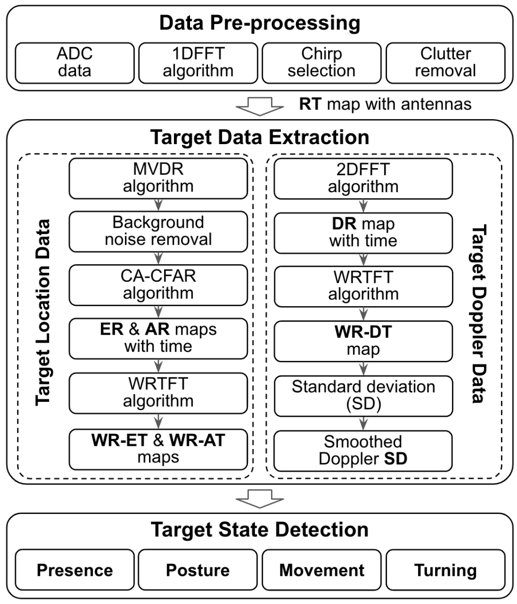

Fig. 2. Data processing and state detection pipeline.

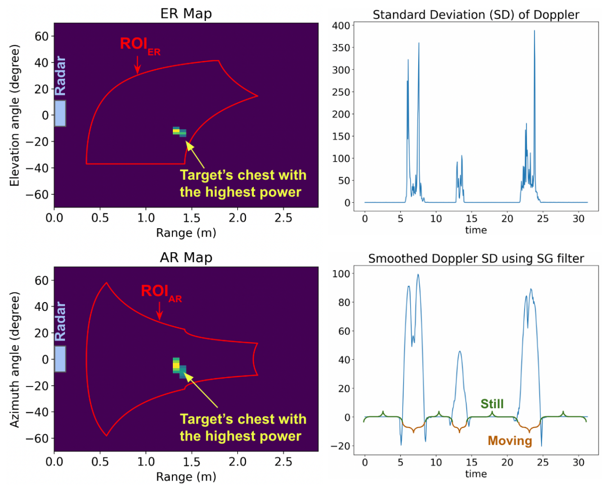

Fig. 3. A target's location data (left) and Doppler data (right).

The latter task is achieved via the Doppler-based computation method. The process starts by applying a 2DFFT on the radar signals that have already been converted into the range domain to facilitate the generation of a Doppler-range (DR) map. Following the 2DFFT, the process advances to the application of WRTFT to get the WR-DT map which shows the Doppler change through time. The standard deviation (SD) is used in combination with the smoothing filter Savitsky-Golay (SG) smoothing filter to facilitate the extraction of the start and end of the detected variations triggered by movements as shown in Fig. 3 (right). The output from this stage serves as a tool for recognizing movement sequences.

(3) Target State Detection. The final stage in the proposed solution is to perform the different state detections, namely on-bed presence, posture, and movement, which are explained in the next subsection.

C. *On-bed State Detection Methods*

Fig. 4 summarize the details including the data used, the functions, and the logic involved in performing these different tasks. Four main modules are used including presence detection, stand/sit/lie posture detection, and sleep posture detection. Details are explained as follows.

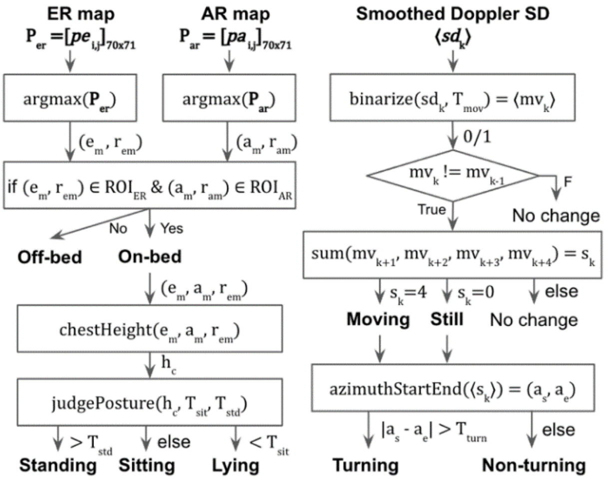

Fig. 4. Target state detection flowchart (radar at head wall).

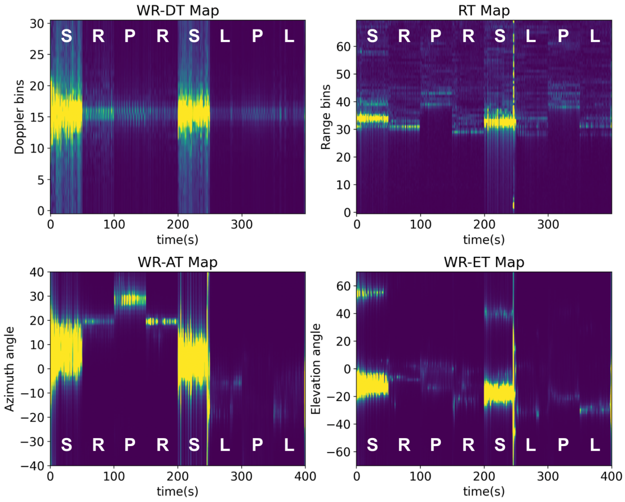

Fig. 5. Sleep postures' maps of WR-DT, RT, WR-AT and WR-ET.

(1) Presence Detection: The primary objective of this module is to identify whether the target is present on the bed or not. Given that the target is within the radar's field of view, the region corresponding to the individual's chest exhibits the greatest power. Consequently, the cells with the highest power levels, denoted as (e_m, r_{em}) and (a_m, r_{am}) in both the azimuth-range (AR) and elevation-range (ER) map (P_{er} and P_{ar}), are recognized as representing the subject's chest. If both of these cells fall within the region of interest (ROI), it is deemed that the target is on the bed. Conversely, if either or both of these cells lie outside the ROI, the target is considered to be out of the bed.

(2) Standing/Sitting/Lying Detection: The detection of the three postures is performed only when the subject is identified as being on bed. In such instances, the values r_{em}, e_m, and a_m obtained through presence detection are subsequently used to calculate the height of the target's chest (h_c) using the formula provided in equation (4) where α is the tilt angle of the radar. The thresholds (T_{std}, T_{sit}) for conducting posture detection are calculated based on the subject's height, employing the standard ratio between height and either shoulder height or shoulder width.

$$h_c = H - r_{em}[\cos(e_m)\cos(a_m)\sin(\alpha) - \sin(e_m)\cos(\alpha)] \quad (4)$$

(3) Movement Detection: A specific period is designated as the no-target phase at the beginning. The average value of the smoothed Doppler SD within this phase is used to establish the threshold for detecting movement, referred to as T_{mov}. Each unit of the smoothed Doppler SD is then compared against this threshold, resulting in the generation of a preliminary movement outcome represented as a sequence called "$< mv_k >$". However, due to the inherent instability of the original signal, an additional algorithm is applied to enhance the performance. This algorithm ensures that the result will only be modified after the system verifies the presence of at least five consecutive changes. The final result is saved in a sequence called "$< s_k >$".

(4) Sleep Posture Detection: Sleep posture detection is specifically applied when the subject is in a lying posture on the bed and remains motionless. To address this objective, our study employed two distinct methods: logic-based and deep learning/DL-based approaches, which are shown in Fig. 6 and Fig. 7, respectively. The logic-based method is to utilize the features of radar data in different, while the deep learning-based is to relies on learning ability with labeled data.

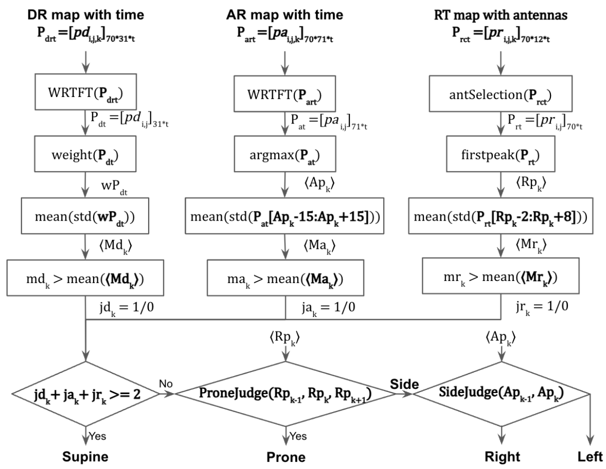

Fig. 6. Sleep posture detection flowchart based on logic.

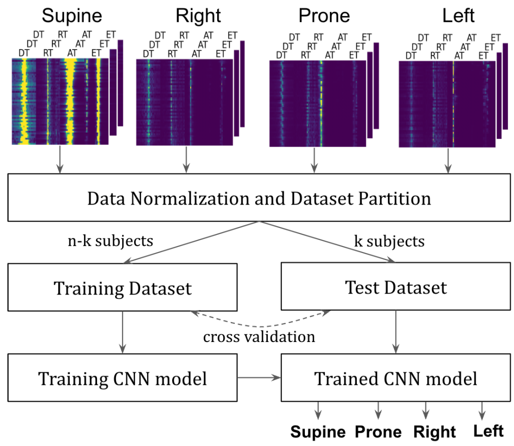

Fig. 7. Sleep posture detection flowchart based on CNN.

The proposed logic involves obtaining the DR and AR maps over time. WRTFT is used to derive the WR-DT and WR-AT grids (P_{dt} and P_{at}). Additionally, the RT grid (P_{rt}) is extracted from a single channel for RT information. After incorporating Doppler information into the DT map through weighted adjustments (resulting in wP_{dt}), a subject location can be determined using the dominant angle bin ($< Ap_k >$) and nearest peak in the range profile ($< Rp_k >$). Power analysis of the WR-DT, WR-AT, and RT maps reveals correlations with breathing strength, quantified by the SD and average power values during each still period ($< Md_k >$, $<$

$Ma_k >, < Mr_k >$). The logical framework identifies supine (S) posture using the mean value of the sleep record as a trigger, distinguishing between side and prone (P) postures based on changes in distance, and separating left (L) and right (R) from side based on changes in azimuth angle.

Fig. 7 illustrates the DL-based approach, which capitalizes on the 2D vector format of the data resembling an image. Given this similarity, Convolutional Neural Network (CNN) known for its proficiency in image recognition is employed. Before initiating the deep learning process, data preprocessing and dataset partition are applied. During preprocessing, the DT, RT, AT, and ET data are normalized individually and then combine them into a unified 2D matrix. As for dataset partitioning, various window sizes (WS), sliding window sizes (SL), and different combinations of the data were experimented. The data from n-k subjects are for training and the remaining k subjects' data are for testing. The subject-wise cross-validation is further conducted to evaluate and compare the accuracy of the parameters and data used.

III. Radar Setting & Experiment Protocols

In this section, a description about the radar parameters used, radar position settings, and three separate experimental protocols are presented.

A. Radar Positions and Parameters

To evaluate the proposed method, the TI-IWR6843ISK-ODS [10] coupled with an acquisition board DCA1000 are adopted in order to collect the raw ADC data. 16 chirps per frame per second is configured for data collection. Each range bin represents to 0.04m according to our configuration. The radar is connected to a desktop PC where TI mmWave Studio software was used to acquire the data and then pass to the solution implemented using Python to perform the processing task. Fig. 8 illustrates the setting of the three radar positions and setting where the experiments took place.

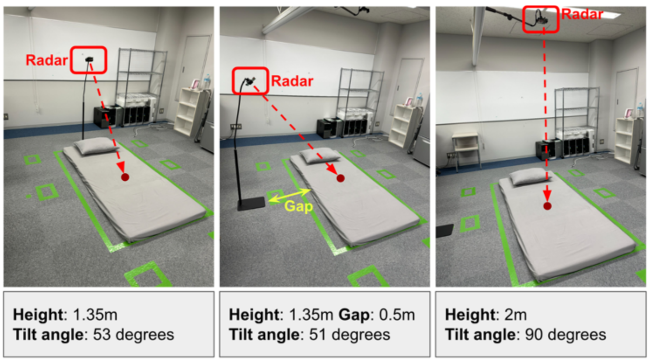

Fig. 8. Radar at head wall, side wall, and ceiling respectively.

B. Experiment Protocols

The experimental procedures were carried out in our laboratory, involving 10 male participants. We devised three separate experiments, each focused on assessing the performance and potential limitations of the distinct aspects of the judgment process: presence, posture, and movement.

(1) Presence Experiment: The subject is asked to sit at locations 01-13 and perform different actions for 10 sec each (staying still, moving head, moving body, moving arm) as shown in Fig. 9. The subject has 5 seconds to transmit between locations. This experiment is repeated once for each radar location (R1: head wall, R2: side wall, and R3: ceiling).

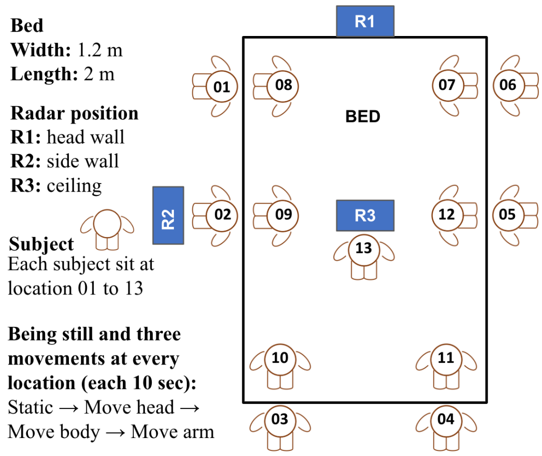

Fig. 9. Presence experiment.

(2) Standing/Sitting/Lying and Movement Experiment: The subject is asked to first stand at locations SD1-SD4 as shown in Fig. 10 while performing different actions for 10 sec each (staying still, moving head, moving body, moving arm), before switching to sitting on bed at locations ST1-ST4 and performing the same group of movement. After sitting on bed, the experiment is switched to lying on bed at location L1-L5, performing the same group of movements, to see the impact of movements to the recognition of postures.

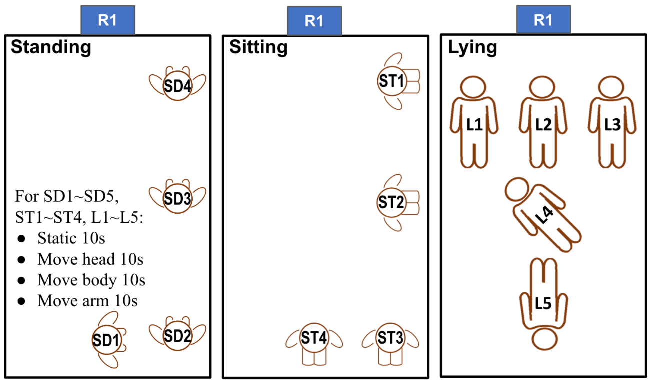

Fig. 10. Standing/sitting/lying posture experiment.

(3) Sleep Posture Experiment: the subject is instructed to assume various postures while lying on the bed. Each posture requires the subject to maintain stillness for a duration of 1 minute. The experiment consists of two primary parts: turning to the right and turning to the left. The turning to the right part includes 1 supine, 2 right side, and 1 prone. Similarly, the turning to the left part comprises 1 supine, 2 left side, and 1 prone posture. Consequently, each posture in the experiment is represented by a 2-minute data segment.

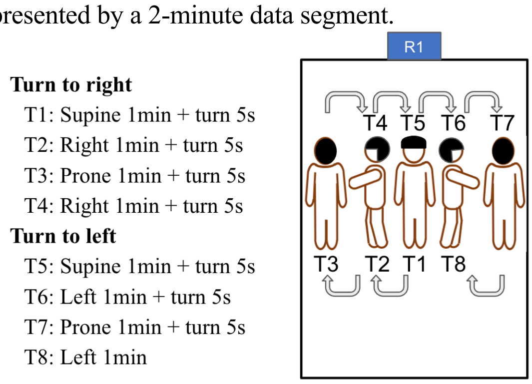

Fig. 11. Sleep posture experiment.

IV. State Detection Result and Discussion

This section presents the results derived from the various experiments conducted for evaluation. The evaluation involves comparing the number of correct detections and calculating various assessment metrics, including precision, F1-score, and analyzing the impact of each condition on the correct detection of presence, posture, and movement.

A. Presence Detection Result

Following the experimental details depicted in Fig. 9, the results from 10 subjects have been collated in Table I. Across all locations inside the bed (07-13), our solution provided a 100% F1-score for presence detection while sitting and performing the different actions with different radar locations proving the reliability of on-bed detection. On the other hand, the detection of off-bed targets shows some limitations at specific locations depending on radar position. When radar is placed at head wall (R1), the performance in locations 02 - 05 achieves good performance, while there is a huge drop for locations 01 and 06 with an F1-score of 18.4% for the latter. This can be attributed to the critical position of these points at the edge of the FoV of the radar triggering multiple cases of false detections, in addition to the unique sitting way for each subject at the edge of the bed which also caused false detections. Switching to side wall (R2), there is a noticeable drop across all outside locations, especially for location 02 which may lay outside or at the edge of the field of view of the radar due to its closeness (sitting in the 0.5 m gap between the bed and the radar as shown in Fig. 8) and a low elevation since radar is at 1.35 m while the chest of the subject while sitting is at 0.6-0.7 m. In addition, and similar to the case of R1, location 01 also gave a poor performance.

TABLE I. Position-Dependent Presence Detection Results

Location	Head Wall		Side Wall		Ceiling	
	Pr %	F1-s %	Pr %	F1-s %	Pr %	F1-s %
01	57.3	72.8	32.4	48.8	48	64.9
02	100	100	5	9.5	75.1	85.8
03	99.2	99.6	78	87.6	93.1	96.4
04	100	100	68	81	88.8	94.1
05	70.92	83	68	81	86	92.5
06	10.1	18.4	98	99	100	100
07	100	100	100	95.5	100	100
08	100	100	100	100	100	100
09	100	100	100	100	100	100
10	100	100	100	100	100	100
11	100	100	100	100	100	100
12	100	100	100	100	100	100
13	100	100	100	100	100	100

When examining the results of detection from ceiling position (R3), the improvement in performance is clear across all locations with a drop only in location 01 which proves to be a limitation for our current detection solution according to the results. The ceiling location allows the radar to have a better view of the bed when comparing to head wall and side wall which explains the improvement in detection for off-bed cases. The analysis of the experimental results across the three radar positions demonstrates the reliability of our solution in determining the subject's presence on the bed. It is worth mentioning that these results are aggregated without considering the various movements performed during the experiments.

B. Movement Impact on Presence Detection

As shown in Fig. 12, the presence detection achieves an F1-score higher than 90% under the impact of the different movements and in all three radar positions. In line with expectations, the result indicates a downward trend in performance transitioning from a still state to motion, with full body or arm movements having the most notable performance drops. The magnitude of head movement is comparatively smaller when compared to body and arm movement, resulting in a relatively smaller drop in performance.

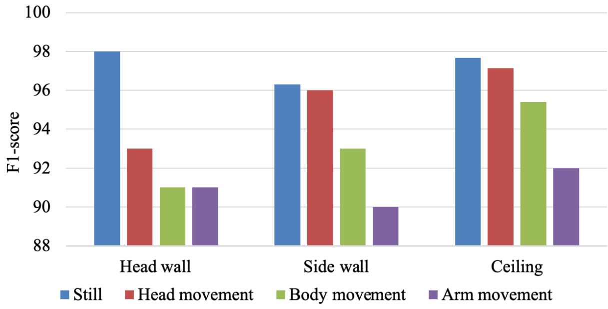

Fig. 12. Impact of motion on presence detection per radar position.

C. Standing/Sitting/Lying Posture Detection Result

Next, the posture detection results are presented with the radar positioned in the head wall position (R1) since it is considered the most practical for a real-world deployment and is less considered in most previous studies which focused mainly on the ceiling position. Among all postures, lying was detected with the highest precision, achieving an impressive F1-score of 99.5%. Both sitting and standing postures were also recognized with over 90% accuracy. Fig. 13 also displays the impact on posture detection performance between still and when moving. The result shows a clear decrease in accuracy when switching from still state into moving across all postures.

Posture	Pr %	F1-s %
Lying	100	99.5
Sitting	100	95.2
Standing	100	91.9

Note: Subject is static.

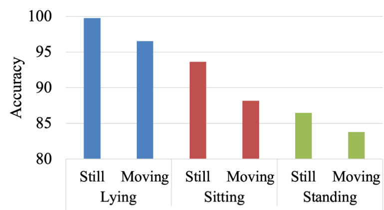

Fig. 13. Detection results in still (left) and accuracy impact in motion (right).

D. Movement Detection Result

From Fig. 14, the accuracy of moving the whole body is understandably higher since it is easier to detect due to the large reflecting surface compared to the arm or the head. In addition to having a relatively smaller reflective area, the movements of the head exhibited by some of the subjects were very small and contributed to the low accuracy results.

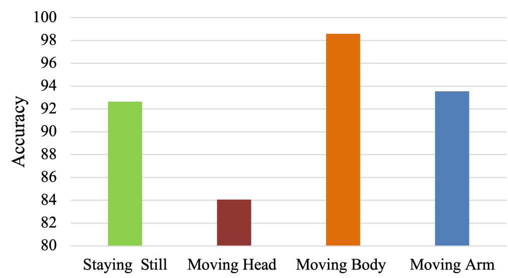

Fig. 14. Detection accuracy of still vs movement actions.

E. Sleep Posture Detection Result

Based on the logical framework outlined in Fig. 6, its performance is first evaluated using 3-category recognition, as depicted in the left confusion matrix in Fig. 15. The results revealed an impressive accuracy of 98.11% for the 3-category recognition based on our logic approach. Notably, all supine postures in the experiment records were correctly identified. However, errors primarily happened in distinguishing prone postures, which were occasionally misclassified as supine. A detailed analysis of each experiment highlighted a correlation with body mass; subjects with higher body mass exhibited more powerful breathing, leading to false recognition of prone as supine. Given the excellent results achieved through 3-category recognition, we extended our analysis to 4-category recognition, as shown in the right confusion matrix in Fig. 15. The overall accuracy for 4-category recognition reached 94.79%. As the proposed logic focuses on distinguishing left and right from side postures, the recognition results for supine and prone remained consistent. However, errors in prone posture recognition also affected the accuracy of left and right recognition, as the logic relies on changes in azimuth angle and previous postures.

In the CNN approach, we trained the model using various window sizes (WS), sliding window sizes (SL), and subject-independent data. The results are presented in the left table of Fig. 16, where D represents the WR-DT map, R denotes the RT map, E signifies the WR-ET map, and A represents the WR-AT map. From the results, it is observed that increasing the window size led to improved performance. Similarly, as the sliding window size increased, the results also demonstrated improvement. Regarding data combination, the DRA combination yielded the best results, surpassing the performance achieved when using all four data sources. After extensive experimentation with WS-wise, SL-wise, and different data combinations, the optimal parameters is identified: a window size of 30 seconds, a sliding window size of 5 seconds, and the DRA data combination, resulting in an accuracy of 94.38%. To provide a comprehensive evaluation of the model, we employed an advanced 5-fold cross-validation approach. The resulting confusion matrix, depicted on the right side of Fig. 16, demonstrates an overall accuracy of 93.25%.

Upon comparing the CNN approach with the logic approach, it is found that the logic approach achieved slightly higher accuracy in posture recognition. However, the CNN approach holds the advantage of real-time applicability, whereas the logic approach requires analysis after recording the entire sleep session. Each approach has its own strengths and limitations, and the choice depends on the specific application requirements.

V. Conclusion and Future Work

This research is focused on a novel on-bed state detection solution leveraging FMCW radar technology. One of the key contributions lies in a unique bed modeling strategy from the radar's viewpoint, facilitating the projection of the Region of Interest (ROI) into AR and ER maps. Additionally, an innovative solution is presented for identifying the on-bed state of individuals by pinpointing chest location. We further achieved simultaneous detection of on-bed presence, motion, posture, and turning. In addition, a comprehensive experimental evaluation is performed to determine the robustness and constraints of our proposed approach.

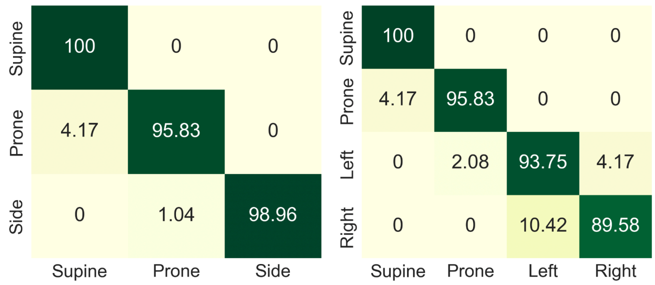

Fig. 15. Logic-based sleep posture detection confusion matrices.

Experiment type	WS	SL	Acc.
WS-wise (DREA)	15s	1s	90.03%
	20s	1s	91.55%
	30s	1s	**92.11%**
SL-wise (DREA)	30s	3s	91.52%
	30s	5s	**93.13%**
DRA	30s	5s	**94.38%**
DRE	30s	5s	87.5%
DR	30s	5s	64.38%
DA	30s	5s	64.38%
D	30s	5s	53.75%
R	30s	5s	77.5%

WS: window size, SL: sliding window size

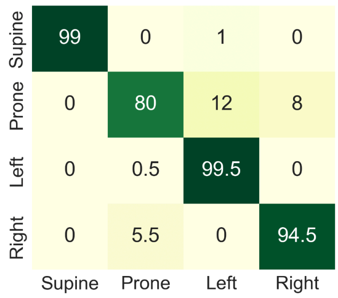

Fig. 16. CNN-based sleep posture detection accuracy and confusion matrix.

On the other hand, currently, the attempts to differentiate when the subject is off-bed yield suboptimal accuracy across all radar positions. Enhancing the off-bed detection logic requires further investigations. Furthermore, our objective is to expand the applicability of the logic for sleep state monitoring across all three radar positions, with a subsequent focus on the most practical position, namely the nightstand. Additionally, considering the prolonged duration of sleep, post-processing can be applied to the deep learning approach.

References

[1] C.J. Lin, T.S. Wei et al., "Bed-exit behavior recognition for real-time images within limited range", Sensors, vol. 22(15), 2022.

[2] J. Clemente, M. Valero, F. Li, C. Wang and W. Song, "Helena: real-time contact-free monitoring of sleep activities and events around the bed", IEEE International Conference on Pervasive Computing and Communications (PerCom), Austin, TX, USA, pp. 1-10, 2020.

[3] Apple, "Apple watch user guide", Accessed on: May 10, 2023. [Online]. Available: https://support.apple.com/guide/watch/track-yoursleep-apd830528336/watchos

[4] N. Carbonaro, M. Laurino et al., "Textile-based pressure sensing matrix for in-bed monitoring of subject sleeping posture and breathing activity", Applied Sciences, vol. 11(6), 2021.

[5] G. Zhang, I.V. Vahia et al., "Contactless in-home monitoring of the long-term respiratory and behavioral phenotypes in older adults with COVID-19: a case series", Frontiers in Psychiatry, vol. 12, 2021.

[6] A. Adhikari, S. Sur, "Argosleep: Monitoring sleep posture from commodity millimeter-wave devices", IEEE INFOCOM, 2023.

[7] Yue, Shichao, et al. "BodyCompass: Monitoring sleep posture with wireless signals", Proceedings of the ACM on Interactive, Mobile, Wearable and Ubiquitous Technologies 4.2, 2020.

[8] T. Zhou, Z. Xia, X. Wang, F. Xu, "Human sleep posture recognition based on millimeter-wave radar", 2021 Signal Processing Symposium (SPSympo), LODZ, Poland, pp. 316-321, 2021.

[9] Y.K. Yoo, C.W. Jung, H.C. Shin, "Unsupervised detection of multiple sleep stages using a single FMCW radar", Appl. Sci. 2023.

[10] E. Turppa, J.M. Kortelainen, O. Antropov, T. Kiuru, "Vital sign monitoring using FMCW radar in various sleeping scenarios", Sensors, vol. 20, 2020.

[11] M. Piriyajitakonkij et al., "SleepPoseNet: Multi-view learning for sleep postural transition recognition using UWB", IEEE Journal of Biomedical and Health Informatics, vol. 25 (4), pp. 1305-1314, 2021.

[12] Texas Instruments, "IWR6843ISK-ODS", Accessed on: Apr 14, 2023. [Online]. Available: https://www.ti.com/tool/IWR6843ISK-ODS.